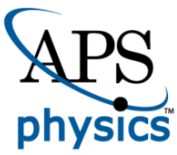

Quantum-Dot-Based Resonant Exchange Qubit

J. Medford, J. Beil, J. M. Taylor, E. I. Rashba, H. Lu, A. C. Gossard, and C. M. Marcus

Phys. Rev. Lett. **111**, 050501 — Published 31 July 2013

DOI: 10.1103/PhysRevLett.111.050501

The Resonant Exchange Qubit

J. Medford[1], J. Beil[2], J. M. Taylor[3], E. I. Rashba[1], H. Lu[4], A. C. Gossard[4], and C. M. Marcus[2]
[1]*Department of Physics, Harvard University, Cambridge, Massachusetts 02138, USA*
[2]*Center for Quantum Devices, Niels Bohr Institute, University of Copenhagen, Universitetsparken 5, 2100 Copenhagen, Denmark*
[3]*Joint Quantum Institute/NIST, College Park, MD, USA*
[4]*Materials Department, University of California, Santa Barbara, California 93106, USA*

We introduce a solid-state qubit in which exchange interactions among confined electrons provide both the static longitudinal field and the oscillatory transverse field, allowing rapid and full qubit control via rf gate-voltage pulses. We demonstrate two-axis control at a detuning sweet-spot, where leakage due to hyperfine coupling is suppressed by the large exchange gap. A $\pi/2$-gate time of 2.5 ns and a coherence time of 19 μs, using multi-pulse echo, are also demonstrated. Model calculations that include effects of hyperfine noise are in excellent quantitative agreement with experiment.

PACS numbers:

As originally conceived, the two-level system that forms the basis of the semiconductor spin qubit is the electron spin itself, with pulsed exchange between two confined electrons forming a two-qubit gate [1]. Generalizations to two-electron [2–6] and three-electron [7–13] qubits make use of multi-electron states as the quantum two-level system. These qubits offer ease of initialization, control, and readout, or speed of operation, in exchange for the complexity of controlling more than one electron per qubit. An attractive feature of the original single-spin proposal is that qubit rotations are implemented as Rabi processes, driven by a small resonant transverse field, rather than Larmor processes, which use pulsed Larmor precession around larger nonparallel fields. Rabi rotations allow narrow-band wiring away from dc, precession rates controlled by the amplitude of the oscillatory field, and straightforward two-axis control (needed for arbitrary transformations) implemented using the phase of the oscillatory field [14, 15].

In this Letter, we introduce a new quantum-dot-based qubit—the resonant exchange qubit—that captures the best features of previous incarnations, with qubit rotations via Rabi nutation using gate-controlled exchange both for the static longitudinal field and the oscillatory transverse field, as described in Ref. [16]. The large exchange field suppresses leakage from the qubit space. However, because rotations are driven by a resonant transverse field, the large longitudinal field does not impose unrealistically fast evolution between qubit states. Moreover, the qubit is operated at a "sweet spot" of the exchange gap, making it insensitive to first order to electrical noise in the detuning parameter [16–19].

The resonant exchange qubit was realized in a triple quantum dot formed by surface gates 110 nm above a two-dimensional electron gas (density 2.6 $\times$ 10^{15} m^{-2}, mobility 43 m^2/Vs) in a GaAs/$Al_{0.3}Ga_{0.7}$As heterostructure [see Fig. 1(a)]. Gate voltages V_l and V_r controlled detuning, $\varepsilon = (V_r - V_r^0)/2 - (V_l - V_l^0)/2$, measured relative to the center of the 111 charge region, while V_m controlled the size of the 111 region (111 and other number triplets denote the charge occupancy of the triple dot) [20]. An adjacent multi-electron quantum dot operated in Coulomb blockade regime served as a radio frequency (rf) charge sensor [21, 22].

Tunneling between adjacent quantum dots gives two exchange splittings, $J_l(\varepsilon)$, associated with the electron pair in the left and middle dots, and $J_r(\varepsilon)$, associated with the electron pair in middle and right dots. Away from zero detuning, defined as the center of 111, the qubit ground state, $|0\rangle = \frac{1}{\sqrt{6}}(|\uparrow\uparrow\downarrow\rangle + |\downarrow\uparrow\uparrow\rangle - 2\,|\uparrow\downarrow\uparrow\rangle)$, connects continuously to a singlet state of the left pair, $|S_l\rangle = \frac{1}{\sqrt{2}}(|\uparrow\downarrow\uparrow\rangle - |\downarrow\uparrow\uparrow\rangle)$ in charge state 201, and to a singlet state of the right pair, $|S_r\rangle = \frac{1}{\sqrt{2}}(|\uparrow\uparrow\downarrow\rangle - |\uparrow\downarrow\uparrow\rangle)$ in charge state 102. [see Fig. 2(a)]. The excited qubit state, $|1\rangle = \frac{1}{\sqrt{2}}(|\uparrow\uparrow\downarrow\rangle - |\downarrow\uparrow\uparrow\rangle)$, maps into triplet states that, in contrast to the singlets, cannot tunnel into charge states 201 or 102. This allows the qubit state to be detected with a charge sensor the distinguishes 201, 111,

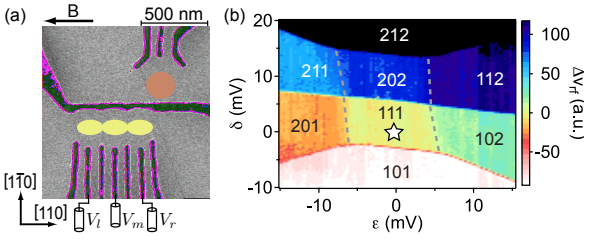

FIG. 1: (a) False color micrograph of lithographically identical device with dot locations depicted; gates are marked in yellow. Gate voltages, V_l and V_r, set the charge occupancy of left and right dot as well as the detuning, ε of the qubit. A neighboring sensor quantum dot is indicated with a larger circle. (b) Triple dot charge occupancy N_l N_m N_r as a function of V_l and V_r in and near the 111 regime; $\varepsilon = (V_r - V_r^0)/2 - (V_l - V_l^0)/2$, $\delta = (V_r - V_r^0)/2 + (V_l - V_l^0)/2 + \gamma(V_m - V_m^0)$. Measurements give $\gamma \sim 3$. The operating position is marked with a star, which is larger than the amplitude of voltage modulation used in rotations.

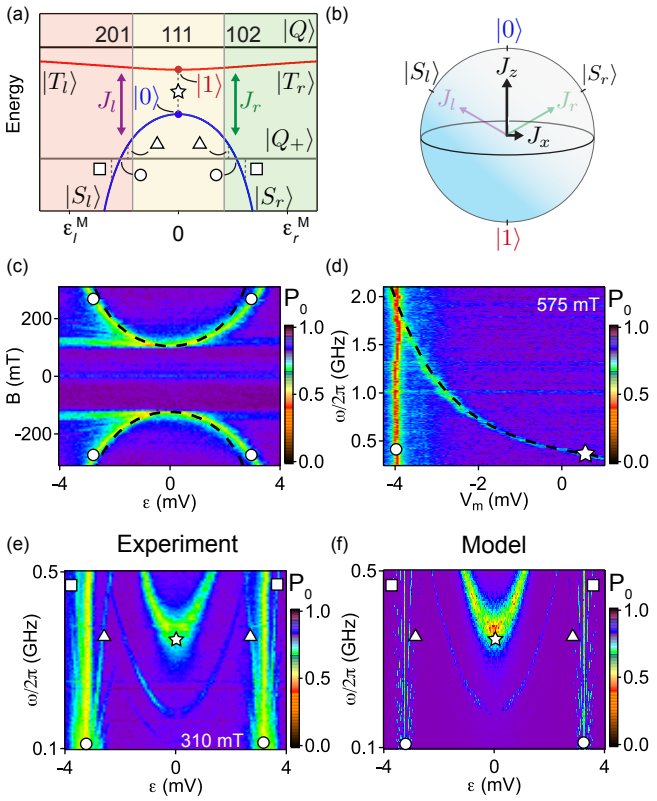

FIG. 2: (a) Energy level diagram for a constant δ. Charge transitions are marked with circles (qubit-$|Q_+\rangle$), triangles (qubit-$|Q_+\rangle$, photon), squares (qubit-$|Q_+\rangle$, photon), and a star ($|0\rangle$-$|1\rangle$) transitions. (b) Schematic of the effects of J_l and J_r on the qubit Bloch sphere (c) The qubit-$|Q_+\rangle$ anti-crossing is mapped out in magnetic field and detuning without an excitation. Dashed line is a model of the exchange splitting for equal tunnel couplings. (d) A sweep of the middle plunger gate at $\varepsilon = 0$ mV and fixed field of 575 mT, demonstrating control of the main qubit transition. The dashed curve is a model of $J_l + J_r$ as a function of $\varepsilon_0 = (V_m - V_m^0)/2$ [23]. (e) At a fixed field of 310 mT, detuning and microwave burst frequency are swept to trace out the spectroscopy of the qubit. (f) A model of qubit evolution in the presence of a microwave excitation and magnetic field gradients between dots in the longitudinal and transverse directions.

and 102. A third state, $|Q_+\rangle = |\uparrow\uparrow\uparrow\rangle$, intersects the qubit ground state at two anti-crossings whose position depends on Zeeman splitting from an external magnetic field. By sweeping the magnetic field, the qubit ground-state energy can be measured as a function of detuning [Figs. 2(a,c)]. The fourth state in Fig. 2(a), $|Q\rangle = \frac{1}{\sqrt{3}}(|\uparrow\uparrow\downarrow\rangle + |\uparrow\downarrow\uparrow\rangle + |\downarrow\uparrow\uparrow\rangle)$, is separated from the qubit states by a sizable gap (half the separation between $|0\rangle$ and $|1\rangle$), suppressing leakage out of the qubit space. The gap to $|Q\rangle$ is deliberately kept large by setting tunneling rates, hence J_l and J_r, to be large throughout the 111 charge region.

Qubit rotations are implemented by applying an oscillatory voltage to gate V_l, which moves the operating point around $\varepsilon = 0$, in turn creating an oscillatory transverse field J_x [see Fig. 2(b)]. When the oscillation frequency ω matches the longitudinal exchange frequency, $J_z/\hbar$ [see Fig. 2(b)], the qubit nutates between $|0\rangle$ and $|1\rangle$. Figure 2(c) maps the positions of the $|Q_+\rangle$ anti-crossings with the lower qubit branch as a function of field and detuning without applied microwaves, along with a model calculation of the exchange splittings J_l and J_r. This spectroscopy is performed by preparing a $|S_r\rangle$ state in 102, then pulsing into 111 for 300 ns before returning to 102 to project the resulting state back onto $|S_r\rangle$.

The data in Fig. 2(d) shows two features, a vertical line corresponding to the crossing of $|Q_+\rangle$ and the center of the lower qubit branch (circle), and a curved feature reflecting a driven oscillation between qubit states $|0\rangle$ and $|1\rangle$, marked with a star. The curved feature shows that the qubit splitting is controlled by gate voltage V_m, here covering a range from 200 MHz to 2 GHz. Using fast gating, we have demonstrated control of this frequency on nanosecond time scales. The dashed line in Fig. 2(d) is a model of $\omega(V_m)$ that assumes a linear dependence of J_l and J_r on V_m.

The resonant exchange qubit can be modeled by the Hamiltonian,

$$\mathcal{H}(\varepsilon) = -J_z\sigma_z/2 - J_x\sigma_x/2, \qquad (1)$$

where $J_z = \frac{1}{2}(J_l(\varepsilon) + J_r(\varepsilon))$ and $J_x = \frac{\sqrt{3}}{2}(J_r(\varepsilon) - J_l(\varepsilon))$, where $\sigma_z = |0\rangle\langle 0| - |1\rangle\langle 1|$ and $\sigma_x = |0\rangle\langle 1| + |1\rangle\langle 0|$ are the Pauli operators of the qubit [see Fig. 2(b)]. Exchange fields $J_l(\varepsilon) = -(\varepsilon + \varepsilon_0)/2 + \sqrt{t^2 + (\varepsilon + \varepsilon_0)^2/4}$ and $J_r(\varepsilon) = (\varepsilon - \varepsilon_0)/2 + \sqrt{t^2 + (\varepsilon - \varepsilon_0)^2/4}$ are modeled in terms of the tunnel coupling, t, which is taken to be the same for both the 201-111 and 111-102 transitions, and $\pm\varepsilon_0$, the detunings of these charge transitions. At $\varepsilon = 0$, this gives $dJ_z/d\varepsilon = 0$ and $dJ_x/d\varepsilon = \frac{\sqrt{3}}{2}(1 - \varepsilon_0/\sqrt{4t^2 + \varepsilon_0{}^2})$. For small detuning, $\varepsilon \ll \varepsilon_0$, J_z is unchanged to first order while $J_x \sim \varepsilon$. This system is equivalent to a spin-1/2 in a large static field with a small transverse field. While J_z is insensitive to detuning noise to first order, it is not insensitive to noise on gate V_m or other gates. However, other gates, including V_m, do not need to operate at high frequency, and so can be heavily filtered.

In Fig. 3, $|S_r\rangle$ is prepared in 102 and adiabatically evolved to $|0\rangle$ at $\varepsilon = 0$, taking care to move rapidly through the $|Q_+\rangle$ anti-crossing. A microwave burst is then applied to V_l for a time τ_B before returning adiabatically to 102 for measurement. The color plot shows the probability, P_0, of detecting the ground state through a charge measurement (see Sec. I, Supplemental Material.) By sweeping frequency and power, we see patterns characteristic of Rabi nutations subject to low frequency noise in the splitting frequency, ω_{01} due to hyperfine gradients (see Sec. VI, Supplemental Information). In the rotating frame, the amplitude of the oscillation gives

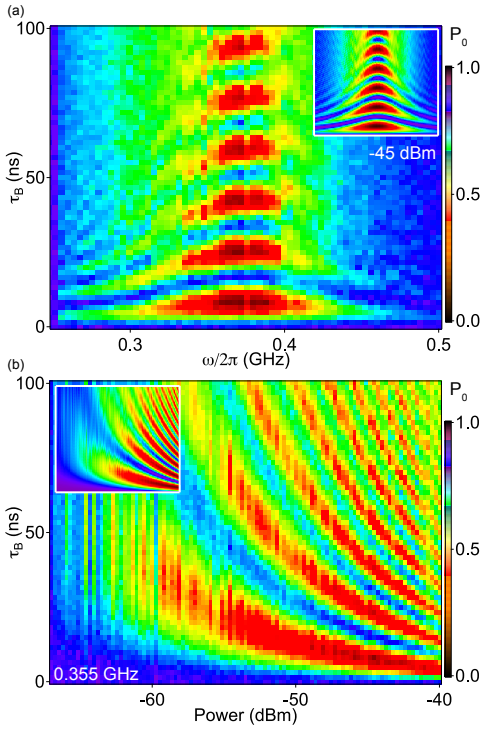

FIG. 3: (a) A Rabi nutation for a -45 dBm (0.45 mV) excitation on the left plunger gate with the detuning biased to the center of the transition [(⋆) in Fig. 2(a,e)] for a time τ_B. (b) A Rabi nutation with a 0.355 GHz excitation on the left plunger gate with the detuning biased to the center of the transition. (insets) A model of this nutation using the exchange profile from Fig. 2(f) and fluctuating longitudinal magnetic field gradients.

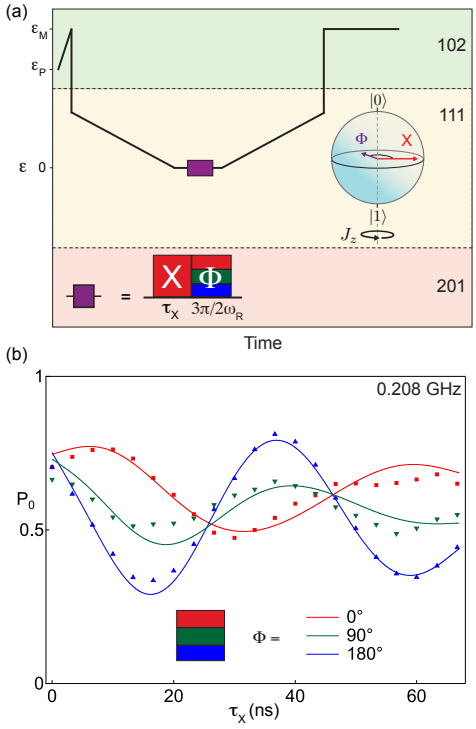

FIG. 4: (a) A schematic of the detuning during a two-pulse sequence, where the first pulse is an X rotation and the second pulse is a rotation around an angle set by the relative phase of the carrier, Φ, as depicted on the Bloch sphere. (b) The qubit readout for a rotation about X, followed by a $\frac{3\pi}{2}$ rotation about an axis Φ, for three different Φ's. The solid lines are fits to the model in Fig. 2(c,d,f) and the insets of Fig. 3.

the strength of the $\hat{x}$ rotation, while the frequency detuning, $\delta = \omega - \omega_{01}$, gives the strength of the $\hat{z}$ rotation. As seen in Fig. 3(b), as the power increases, effects of δ errors due to hyperfine gradients decrease. At $\omega_{01}/2\pi = 0.355$ GHz, the nutation frequency scales with voltage as $\mathrm{d}\Omega_R/\mathrm{d}V_l \sim 2\pi \times 70$ MHz/mV. This scaling increases with $\mathrm{d}J_x/\mathrm{d}\varepsilon$, which grows as the 111 region is shrunk ($\varepsilon_0 \to 0$) to increase ω_{01}. At $\omega_{01}/2\pi = 1.98$ GHz, this scaling was measured to be $\sim 2\pi \times 5$ GHz/mV, demonstrating a way to increase coupling to external voltages.

On resonance in the rotating frame, the Hamilton takes the form $\mathcal{H}_{\mathrm{rf}} = \cos(\Phi)\sigma_x + \sin(\Phi)\sigma_y$, where Φ is the relative phase of the carrier wave with respect to the first pulse incident on the qubit. Controlling phase relative to the initial pulse thus allows full two-axis qubit control. To test the qubit response, we prepare a $|0\rangle$ and drive a rotation on resonance for a time τ_{x}, then apply a second pulse at relative phase Φ to drive a $3\pi/2$ rotation in a time $3\pi/2\omega_{\mathrm{R}}$. Figure 4 shows data for $\Phi = 0°$, 90°, and 180°, along with model curves using an optimized, though reasonable, value for hyperfine couplings as a fit parameter.

Phase control was sufficient to implement a CPMG dynamical decoupling sequence, where π-pulses are applied along the $\hat{y}$ axis in the rotating frame, partially decoupling rotation errors [15]. Figure 5 shows resulting coherence time, T_2, for CPMG sequences up to 64 π-pulses, which gave $\mathrm{T}_2 = 19 \pm 2\,\mu$s. Values for T_2 were extracted from Gaussian fits to $P_0(\tau_{\mathrm{D}})$, where τ_{D} is the total dephasing time (see inset of Fig. 4). Between 2 and 16 pulses, the scaling of coherence time with (even) pulse number, n_π, appears well described by the power-law, $\mathrm{T}_2 = A(n_\pi)^\gamma$, where $\gamma = 0.84 \pm 0.05$. Within a classical power-law noise model [24, 25] implies $S(\omega) \sim \omega^{-\beta}$ with a $\beta = 5 \pm 1$. The inconsistency of this result with recent studies of electrical noise in the singlet-triplet qubit, where $\beta \sim 0.7$ [26], may reflect first-order insensitivity of the resonant exchange qubit to detuning noise. However, a detailed model for dynamical decoupling that distinguishes voltage noise from hyperfine noise has not been developed to date. Moreover, pulse sequences designed to decouple hyperfine noise for exchange-only qubits [27] may also be adaptable to the resonant exchange qubit.

For $n_\pi > 16$, $\mathrm{T}_2(n_\pi)$ falls below the steep power-law, and appears to saturate around 20 μs. The measured T_1 for a splitting $\omega_{01}/2\pi = 0.33$ GHz was $\sim 40\,\mu$s, and

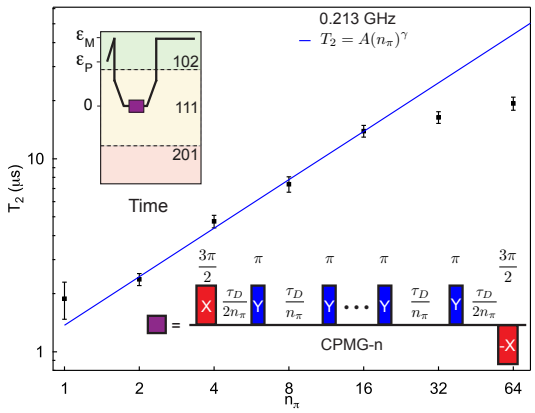

FIG. 5: T_2 for various orders of CPMG-n, were each sequence contains n π rotations about y, as depicted in the lower inset. The upper inset depicts the detuning sequence for this experiment. We found that up to $n = 16$, the even number of pulses was well described by $T_2 = A(n_\pi)^\gamma$, where $\gamma = 0.84 \pm 0.05$. This translates to a power spectral density of $S(\omega) \sim \omega^{-\beta}$, where $\beta = 5 \pm 1$.

decreased monotonically with increasing ω_{01}, consistent with phonon-based relaxation, which suggests that T_1 was not limiting T_2 at $\omega_{01}/2\pi = 0.2$ GHz. Pulse errors are likely limiting T_2 in this measurement, though extending coherence much longer will require extending T_1.

In summary, we have introduced and demonstrated the operation of a new quantum-dot-based qubit that uses exchange for both the longitudinal and oscillatory transverse fields. A large exchange gap prevents state leakage, and the operating point is insensitive to first order to fluctuations in gate-controlled detuning. Two-axis control and a large ratio ($\sim 10^4$) of coherence time to gate operation time were demonstrated. Implementation of a two-qubit gate [16, 28] is next experimental challenge.

Acknowledgements.—Research was supported in part by the Office of the Director of National Intelligence, Intelligence Advanced Research Projects Activity (IARPA), through the Army Research Office grant W911NF-12-1-0354. We also acknowledge support from the National Science Foundation Materials World Network Program, Harvard University, the Villum Foundation, and the Danish National Research Foundation, DARPA MTO and the NSF Physics Frontier Center at the JQI. We thank Maja Cassidy, Oliver Dial, David DiVincenzo, Andrew Doherty, Mark Gyure, Bert Halperin, Ferdinand Kuemmeth, Thaddeus Ladd, and Arijeet Pal for useful discussions.

[1] D. Loss and D. P. DiVincenzo, Phys. Rev. A **57**, 120 (1998).

[2] J. R. Petta, A. C. Johnson, J. M. Taylor, E. A. Laird, A. Yacoby, M. D. Lukin, C. M. Marcus, M. P. Hanson, and A. C. Gossard, Science **309**, 2180 (2005).

[3] J. M. Taylor, H.-A. Engel, W. Dür, A. Yacoby, C. M. Marcus, P. Zoller, and M. D. Lukin, Nature Physics **1**, 177 (2005).

[4] C. Barthel, D. J. Reilly, C. M. Marcus, M. P. Hanson, and A. C. Gossard, Phys. Rev. Lett. **103**, 160503 (2009).

[5] S. Foletti, H. Bluhm, D. Mahalu, V. Umansky, and A. Yacoby, Nature Phys. **5**, 903 (2009).

[6] M. D. Shulman, O. E. Dial, S. P. Harvey, H. Bluhm, V. Umansky, and A. Yacoby, science **336**, 202 (2012).

[7] D. P. DiVincenzo, D. Bacon, J. Kempe, K. B. Whaley, and G. Burkard, Nature **408**, 339 (2000).

[8] L. Gaudreau, S. A. Studenikin, A. S. Sachrajda, P. Zawadzki, A. Kam, J. Lapointe, M. Korkusinski, and P. Hawrylak, Phys. Rev. Lett. **97**, 036807 (2006).

[9] L. Gaudreau, A. Kam, G. Granger, S. A. Studenikin, P. Zawadzki, and A. S. Sachrajda, Appl. Phys. Lett. **95**, 193101 (2009), ISSN 0003-6951.

[10] E. A. Laird, J. M. Taylor, D. P. DiVincenzo, C. M. Marcus, M. P. Hanson, and A. C. Gossard, Phys. Rev. B **82**, 075403 (2010).

[11] L. Gaudreau, G. Granger, A. Kam, G. C. Aers, S. A. Studenikin, P. Zawadzki, M. Pioro-Ladrière, Z. R. Wasilewski, and A. S. Sachrajda, Nature Phys. **8**, 54 (2011).

[12] J. Medford, J. Beil, J. M. Taylor, S. D. Bartlett, A. C. Doherty, E. I. Rashba, D. P. DiVincenzo, H. Lu, A. C. Gossard, and C. M. Marcus, arXiv preprint arXiv:1302.1933[cond-mat.mes-hall] (2013).

[13] F. R. Braakman, P. Barthelemy, C. Reichl, W. Wegscheider, and L. M. K. Vandersypen, arXiv preprint arXiv:1303.1034[cond-mat.mes-hall] (2013).

[14] C. P. Slichter, *Principles of Magnetic Resonance* (Springer-Verlag, Berlin, 1989).

[15] L. M. K. Vandersypen and I. L. Chuang, Rev. Mod. Phys. **76**, 1037 (2005).

[16] J. M. Taylor, V. Srinivasa, and J. Medford, arXiv preprint arXiv:1304.3407 [cond-mat.mes-hall] (2013).

[17] J. Koch, T. M. Yu, J. Gambetta, A. A. Houck, D. I. Schuster, J. Majer, A. Blais, M. H. Devoret, S. M. Girvin, and R. J. Schoelkopf, Phys. Rev. A **76**, 042319 (2007).

[18] J. A. Schreier, A. A. Houck, J. Koch, D. I. Schuster, B. R. Johnson, J. M. Chow, J. M. Gambetta, J. Majer, L. Frunzio, M. H. Devoret, et al., Phys. Rev. B **77**, 180502 (2008).

[19] H. Paik, D. I. Schuster, L. S. Bishop, G. Kirchmair, G. Catelani, A. P. Sears, B. R. Johnson, M. J. Reagor, L. Frunzio, L. I. Glazman, et al., Phys. Rev. Lett. **107**, 240501 (2011).

[20] (V_l^0, V_m^0, V_r^0) = (-588 mV, -452 mV, -145 mV).

[21] D. J. Reilly, C. M. Marcus, M. P. Hanson, and A. C. Gossard, Appl. Phys. Lett. **91**, 162101 (2007).

[22] C. Barthel, M. Kjærgaard, J. Medford, M. Stopa, C. M. Marcus, M. P. Hanson, and A. C. Gossard, Phys. Rev. B **81**, 161308(R) (2010).

[23] The theory curve is a plot of $\omega_{01} = \left(-\beta(V_m - V_m^0) + \sqrt{4t^2 + \beta^2(V_m - V_m^0)^2}\right)/4\hbar$, where β = 20 μeV/mV, t = 16.9 μeV, and V_m^0 = -4.05 mV. A constant tunnel coupling was used here rather than a Gaussian dependent tunnel coupling, because V_l and V_r were constant.

[24] Ł. Cywiński, R. M. Lutchyn, C. P. Nave, and S. Das Sarma, Phys. Rev. B **77**, 174509 (2008).
[25] J. Medford, L. Cywiński, C. Barthel, C. M. Marcus, M. P. Hanson, and A. C. Gossard, Phys. Rev. Lett. **108**, 086802 (2012).
[26] O. E. Dial, M. D. Shulman, S. P. Harvey, H. Bluhm, V. Umansky, and A. Yacoby, arXiv preprint arXiv:1208.2023 (2012).
[27] G. T. Hickman, X. Wang, J. P. Kestner, and S. Das Sarma, arXiv preprint arXiv:1303.6950 [cond-mat.mes-hall] (2013).
[28] Andrew C. Doherty, Matthew P. Wardrop, arXiv preprint arXiv:1304.3416 [cond-mat.mes-hall] (2013).